APPLICATIONS OF MAGNETIC RESONANCE IMAGING IN SPECIAL CORE ANALYSIS STUDIES

J. Lewis A. Williams*, Paulinus M. Enwere, John S. Archer**, David G. Taylor*.**

* University of Surrey,
** Imperial College of Science and Medicine

Abstract Computerised tomography (CT) scanning has been extensively used in the petroleum industry for measurement and imaging of saturation distributions in core floods. So far, the majority of applications have used X-Ray CT scanning, which essentially "sees" the character of the heterogeneous rock and the position of "doped" (added contrast) fluids. A number of processes other than X-Ray scanning lend themselves to tomographic imaging and one of the most promising is nuclear magnetic resonance imaging (NMRI or MRI for short).

The MRI technique, which "sees" the fluids in the pore spaces rather than the rock, is shown to have a number of important complementary advantages over other imaging methods. The results of experimental studies have shown factors that help to discriminate between different fluid species, and to quantify saturation distributions in static and dynamic conditions in cores. The technique has a particular advantage in enhanced oil recovery (EOR) core studies in that it can be made molecular species specific and can be used to image simultaneously the distributions of oil and water and the distribution of EOR additives. From preliminary experiments it appears that there is a potential for high resolution MRI, down to micro scale, which could lead to fundamental and detailed study of entrapment and mobilisation of residual fluids in porous systems.

INTRODUCTION

The prediction of reservoir performance by use of reservoir simulation models is an important area of modern reservoir management. It is quite obvious that the validity of such predictions is inherently related to the quality of the reservoir description utilised to develop the model, and to the characterisation of flow behaviour in the heterogenous pore spaces. Much of the information about flow of oil, gas and water in reservoir rocks is derived from laboratory investigations conducted with 'representative' core samples. "Special Core Analysis" data thus provides a significant input to reservoir simulation, and quite correctly its validity should be questioned. Amongst the questions will be concern about sample wettability and its influence on fluid distribution, concern about the competing capillary, viscous and gravity forces, and, of course, concern about the heterogeneity of the sample and validity of the fluids to represent in situ reservoir conditions. Most laboratory flow tests are designed to eliminate gravity forces and they result in 1-D displacement under viscous-capillary control. Interpretation of test results tend to invoke the concept of a diffuse flow condition and tend to ignore dynamic capillary pressure gradients. Such interpretation may lead to gross error in development of relative permeability relationships which are used in simulators under full viscous/capillary/gravity force controls to develop fractional flow forecasts. There is a pressing need to evaluate the results of appropriate laboratory displacement tests in the light of knowledge about saturation distribution and saturation gradients in the heterogeneous core flood. History matching procedures for validating core flood simulators already exist (Archer, 1986) but their use has been limited by a general lack of knowledge concerning the fluid displacement processes within the core.

In recent years there has been an advance in 2-D interpretation of saturation distribution in cores utilising X-Rays (Hove et al, 1987; Withjack, 1987) and now using nuclear magnetic resonance (NMR). These techniques are more powerful than the earlier 1-D imaging methods involving microwaves (Parsons, 1975), VHF electrical properties (Davis, 1987), radioactive tracers (Josendal et al, 1952). The 2-D imaging methods are based on computer aided creation of 'images' of saturation measurements. The application of methods utilizing X-Rays is based on the transmission of an X-Ray beam through the core sample. The difference in the attenuation coefficients of rock, fluid and gas phases gives image contrast. To be able to visualize a displacement in a porous medium there must be a sufficient difference in attenuation coefficients of the fluids. This is generally

the case for gas-liquid systems, but not for oil-water systems. Often doping agents such as sodium iodide are added to one of the fluid phases to increase the X-ray attenuation and thereby improve the image contrast (Hove et al, 1987). To enhance the visualisation of fluid saturation changes through time a base image of the rock matrix taken prior to fluid injection can be subtracted from the experimental flow images. Work to date on X-Ray CT imaging has been very significant in demonstrating sample heterogeneity and the likelihood of poorly distributed fluids, which may negate assumptions made in simulator calculations. The limitations of the technique appear to reside in resolution of saturation, particularly where interests may lie at pore scales.

Nuclear magnetic logging has long been utilised to measure residual oil in reservoir rocks (Robinson et al, 1974). Even earlier, porosity and permeability of sandstones were studied using pulsed NMR (Timur, 1969). This area of work has been extended (Kenyon et al, 1986). NMR has been applied to direct core measurement to estimate some basic rock properties. MRI, initiated by Lauterbur (1973), provides the possibility of studying the spatial distribution of porosity, pore size and fluid saturation in core plugs. Three dimensional visualisation of the fluids in porous rock is possible down to the micro scale.

Magnetic resonance imaging (MRI) can measure a multiplicity of in core parameters of which the most appropriate are, fluid concentration, chemical shift, nuclear spin-lattice relaxation (T_1) and nuclear spin-spin relaxation (T_2), and fluid flow rates. By comparison with CT scanning the rock core and sample holder do not produce detectable magnetic resonance signals, they are invisible to MRI study of fluids. There are several MRI methods which distinguish oil from water. Chemical Shift Imaging (CSI) is particularly suitable as it is molecular species specific and sufficiently sensitive to distinguish oil from water inside certain rock cores. The relaxation parameters T_1 and T_2 are sensitive to the physical interaction of the fluids with the pore surface.

PRINCIPLE OF MAGNETIC RESONANCE IMAGING

The theory of nuclear magnetic resonance is described in several texts (Farrah and Becker, 1971; MacLauchlan, 1972; Abragam, 1961). An appropriate reference to NMR theory will be made in this paper, and the underlying principle of nucleus excitation and its resulting effect are briefly noted in the Appendix.

The nucleus of certain atoms, particularly hydrogen, has a nuclear moment which interacts with a magnetic field. When nuclei of hydrogen atoms (^1H) contained in water and oil are placed in a magnetic field and excited with a radiofrequency

(rf) pulse of short duration (microseconds), there follows a transient signal which is detected in a coil placed around the rock sample containing the fluids. The amplitude and frequency of this signal gives information on the local chemical and physical environment of the nuclei. Figure 1 shows the arrangement of the rf coil, and some samples. This assembly is placed in the very homogeneous field of the superconducting magnet to excite the nuclei.

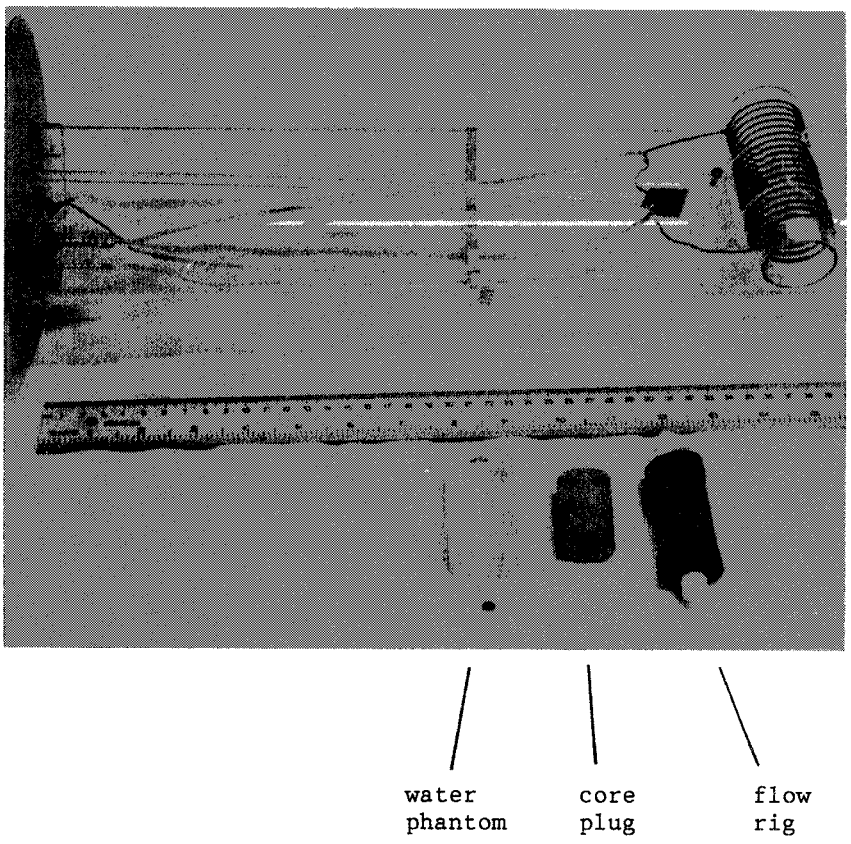

FIGURE 1 Rf coil arrangement and some samples

By applying a series of magnetic field gradient pulses and rf pulses in defined ways, it is possible to select a slice of the sample and spatially localize the signal spectra from small volumes of the slice. These sample volumes are known as voxels. The voxel size is determined by the gradient strength and rf pulse magnitude. For our system the voxel size is approximately 0.9 x 0.9 x 4.5mm. The difference in molecular environment between ^1H in oil and those in water give rise to a very small change in resonance frequency referred to as chemical shift. This difference is about 3.7 parts per million (ppm). By analyzing the frequency components of the NMR signal from a sample of oil and water it is possible to produce an NMR spectrum, which depicts signal intensity versus chemical shift. The signal intensities are proportional to the number of protons in the respective fluids. Hence the quantities of oil and water can be deduced. By combining spatial localisation and spectral analysis techniques chemical shift imaging (CSI) provides a chemical shift spectrum per sample voxel (Hall, 1986 and 1987).

Figure 2a shows an example voxel spectrum from a 1-D chemical shift image of a Portland Limestone core saturated in n-decane and distilled water. The spectrum shows signal amplitude (A) in relative units versus frequency in Hertz (Hz). The natural linewidth of the bulk oil and water fluids measured with our system is less than two Hertz (0.2ppm). The lines are considerably broadened by the rock-fluid interactions.

The oil-water spectral lines can be deconvolved provided that the linewidth does not exceed the line separation. The area under each line is related to the amount of that fluid phase in the voxel. If the complete spectrum is integrated this value is a function of the total fluid concentration (allowance may be made for relaxation rates). If the individual lines are integrated the oil and water concentrations can be evaluated per voxel. Our one dimensional (1-D) technique distinguishes 64 voxels, and the 64 associated chemical shift spectra, per image slice. By deconvolving and integrating the spectral lines, total fluid, oil and water profiles can be produced along the core length. In two dimensional (2-D) Chemical Shift Imaging the distributions correspond to 2-D fluid maps with 64 x 64 resolution.

The presence of magnetic material in the core plug can significantly broaden the linewidths, sandstones are noted for this (Edelstein, 1988). An example voxel spectrum from Lochaline sandstone saturated in oil and water is shown in Figure 2b.

Since gas does not produce a detectable NMR ^1H signal gas distributions will have zero contrast and they can be investigated using image subtraction in a manner similar to that adopted for X-Ray CT scanning.

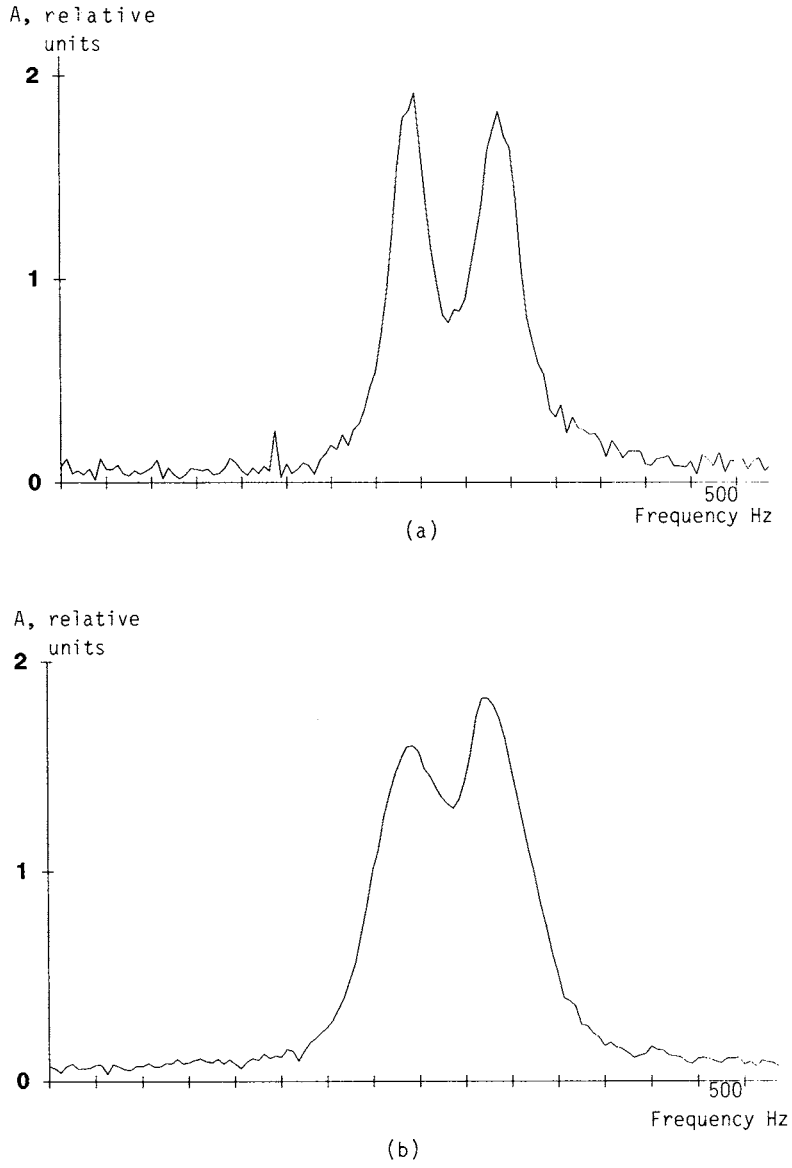

FIGURE 2 Voxel spectra of n-decane and water in (a) Portland limestone core; (b) Lochaline sandstone core.

IMAGING SYSTEM AND EXPERIMENTAL MATERIALS

An MRI system at the University of Surrey was used in this study which comprises a 0.4 Tesla Oxford Instruments magnet (7" bore) and an SMIS Imaging Console.

The 2-D Chemical Shift Imaging (CSI) sequence utilised is illustrated in the Appendix Figure 12. The production of 1-D images or profiles is facilitated by removing the phase encoding gradient in the y-direction. The spatial resolution achieved with the present unit has been verified by calibration to be 0.94 x 0.94 x 4.5 mm.

The rock core plugs were 25.4mm (1") diameter and 50.8mm (2") or less in length. Both limestone and sandstone porous, permeable rocks were utilised. Samples were obtained from outcrops. The limestone was Portland Limestone with a porosity around 12% and a plug permeability of 30md. The sandstone utilised came from Lochaline and was a high quartz sand from a shallow marine depositional environment. Characteristic plug porosities and permeabilities were 20% and 3000md respectively. In addition some work has been conducted using glass bead packs.

The images may be taken in both the axial and longitudinal directions. In the imaging of displacement behaviour we have, at this stage, been mainly interested in the longitudinal plane using the 1-D and 2-D processes. The main control here is a balance between velocity of fluid advance and imaging speeds. It is obvious that 1-D profile images will be less time consuming than 2-D or 3-D imaging. All experiments were conducted at ambient conditions.

The relaxation times T_1 and T_2 for bulk fluids in glass bead packs are shown in Table 1. Similarly, linewidth results for a variety of limestone and sandstone samples which were screened are shown in Table 2.

EXPERIMENTAL INVESTIGATIONS

The MRI technique appears to have the capability to distinguish between fluid species. The rock is effectively transparent with regard to signal interpretation. The resulting 1-D fluid maps derived from the CSI technique should be representative of fluid distribution. However, the CSI technique is based on the assumption that the oil and water spectral lines are resolvable.

The preliminary investigations were aimed at identifying the possibilities of detecting immiscible fluid boundaries, porosity distribution as evidenced from fluid distribution, and saturation gradients during flow.

TABLE 1 Relaxation times, T_1 and T_2 for Bulk Fluids in Glass Bead Packs

Sample	Filename	T_2/ms	T_1/ms
Decane	D	408	1247
Water	W	1780	2460
Water in glass bead packs	W4	488	1010
	W6	421	862
	W9	305	556
Brine in glass bead packs	B4	583	1020
	B6	361	842
	B9	268	536
Decane in glass bead packs	D4	334	1360
	D6	278	1240
	D9	288	1330
Sandstone (clashach)	D	-	496
	B	104	108
	W	125	174

Glass bead sizes

Bead type	dia/mm
4	0.85-1.23
6	0.65-0.75
9	0.29-0.42

TABLE 2 Linewidths and T_2* measurements for selected core plug samples

Rock No.	Code /ms	Rock Type /ppm	linewidth $\nu_{1/2}$
Clashach	1-0	Sandstone	5.0
Birkams	19'-1	Sandstone	18.6
Springwell	17-4	Sandstone	18.6
Crosland Hill	16-5	Sandstone	7.4
Blaxter	15-7	Sandstone	6.6
Dolington	15-8	Sandstone	5.3
Lochaline	1-1	Sandstone	3.1
Gebdykes	18'-2	Limestone	7.4
Portland	21"-5	Limestone	2.9
Monks Park	21'-2	Limestone	4.6
Guiting	2.0	Limestone	12.4
Raisby	18'-9	Limestone	5.3
Barton	15-11	Limestone	7.1

Discrimination between different chemical species was also an important area of interest. From a reservoir engineering standpoint it was considered an exciting opportunity to try and deduce capillary and gravity effects on saturation gradients and thereby obtain greater insight into the full form of the fractional flow equation. Through such a route, proper scaling of force ratios for use in reservoir simulation modelling may be obtained.

RESULTS AND DISCUSSION

Figure 3 shows three profiles; (a) is doped water in a plastic canister of equivalent size to a core sample; (b) is pure distilled water in a core plug of Portland Limestone (12% porosity, 30md permeability); and (c) is the profile of a saturated Lochaline sandstone core (20% porosity, 3000 md permeability). The amplitude of the fluid profile V is proportional to the fluid concentration. The profiles (b) and (c) show the difference between the fluid distribution in a homogeneous and heterogeneous rock. The uniformity of the Lochaline sandstone sample (Figure 3c), was apparent and could have passed for homogeneous sample in routine and special core analysis.

Pure water has an extremely narrow natural linewidth and correspondingly long transverse and longitudinal relaxation rates with our system these have been measured as T_1 = 2.5 seconds T_2 = 1.8 seconds (Table 2). The water sample in the canister was doped with manganese chloride to mimic the line broadening effect of the rock matrix. The linewidth is characterised by T_2*. Water in a Portland Limestone core has a T_2* = 0.06 seconds (Table 2). The distinction between natural linewidth and the transverse relaxation rates T_2 and T_2* is explained in the Appendix A.1.1. Since the core plugs have only 12% and 20% porosity, and the tube 100% porosity the amplitudes of the profiles are on different scales.

The bulk fluid profile demonstrates the uniformity of the radio frequency field and the end response of the coil. Clearly from the profile of the Portland limestone core plug the local porosity varies greatly from voxel to voxel. This local porosity variation determined from the NMR profile has been fitted to a normal distribution with average 12% standard deviation 0.5%.

In a further experiment the detection of two immiscible fluids was simulated. In order to eliminate capillary imbibition effects the base line experiment was conducted in the following manner:

A core plug taken from the Portland limestone was cut into two halves. One half was fully saturated in n-decane and the other half in distilled water. Both halves were butted together and immediately imaged in both 1-D and 2-D.

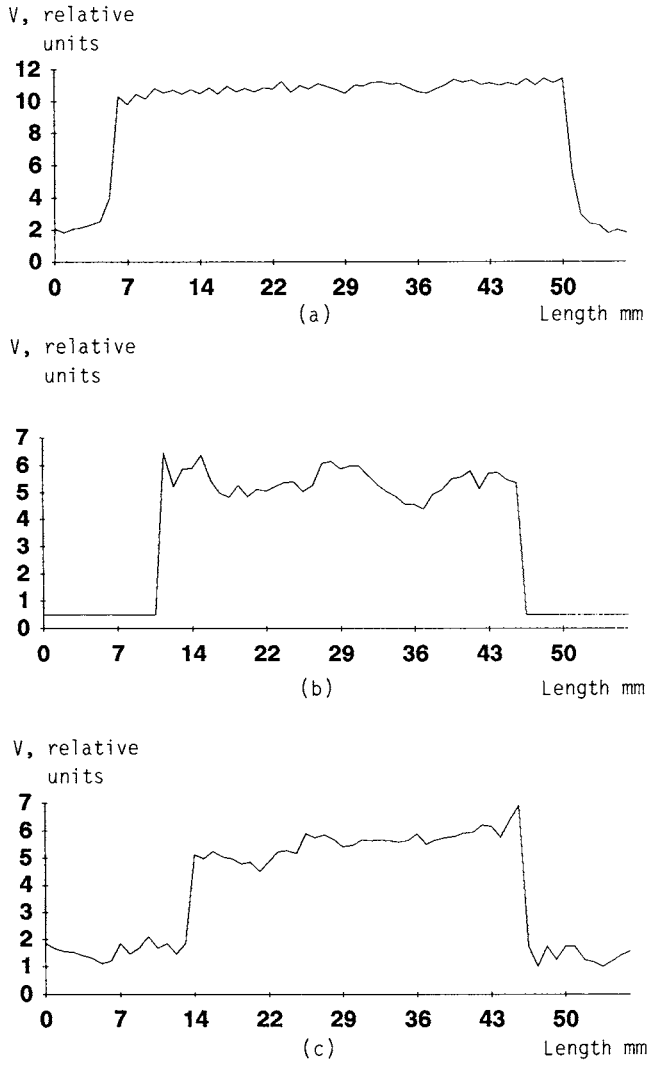

FIGURE 3 1-D total fluid profiles (a) canister of doped water; (b) 100% water saturated Portland Limestone; (c) 100% water saturated Lochaline sandstone core.

Profiles of the total fluid and the individual components are shown in Figure 4 side by side with the corresponding 2-D distributions for comparison. The two phases are clearly distinguished. This preliminary imaging validated our line fitting integration technique as the oil profile was observed to be low in the half containing water and vice versa. This also formed the basis for flood front tracking discussed later. Fluid contents determined by the 1-D and 2-D CSI are in good agreement with each other and with the material balance values.

Other Portland limestone plugs, fully saturated with distilled water and n-decane of known proportions, were also imaged, in cross-sectional 'slices' 4-5mm thick. Non-porous clusters of rock matrix and large sand grains were seen as dark patches with brighter areas of the image depicting higher fluid concentrations.

A series of desaturation experiments was attempted with the Portland limestone plugs. The 100% water saturated plug was imaged, and then spun in a centrifuge for 3 hours at 2300rpm until the weight of the saturated core plug could not be further reduced. The core had an irreducible water saturation of 0.35 PV determined by Mass Balance. The irreducible water signal was detected in the presence of air and the fluid distribution successfully imaged. However, the linewidth was broadened by a factor of two and echo signal was significantly lower than the Mass Balance figures predicted. The detection time of the echo signal was 40ms after excitation. Signals from fluid trapped in small pores decay rapidly since significant surface interactions in the small pores have caused a notable increase in linewidth. Gas-liquid distributions can be studied with MRI in this manner, by image subtraction. The experiment would be improved by reduction in detection time and signal calibration.

The NMR literature has evidence of residual fluid investigations (Robinson et al, 1974) and Edelstein, (1988) has reported short detection times down to 5ms echoes.

The saturation distribution of oil and water fluids was studied with a model system. A homogeneous glass bead pack was flooded with several PV of distilled water, and subsequently 0.45 PV of n-decane, and immediately imaged. The profiles and 2-D images are shown in Figure 5, and representative spectra drawn to scale from pixels 1, 2, 3 and 4 of the 2-D chemical shift data set are shown in Figure 6. The spectra are well separated and the relative proportions of water and n-decane calculated from the areas under the spectral lines agree with expected levels in this model system. The low signal from the oil is due to its longer T^1 relaxation rate, and the preferential water wettability of

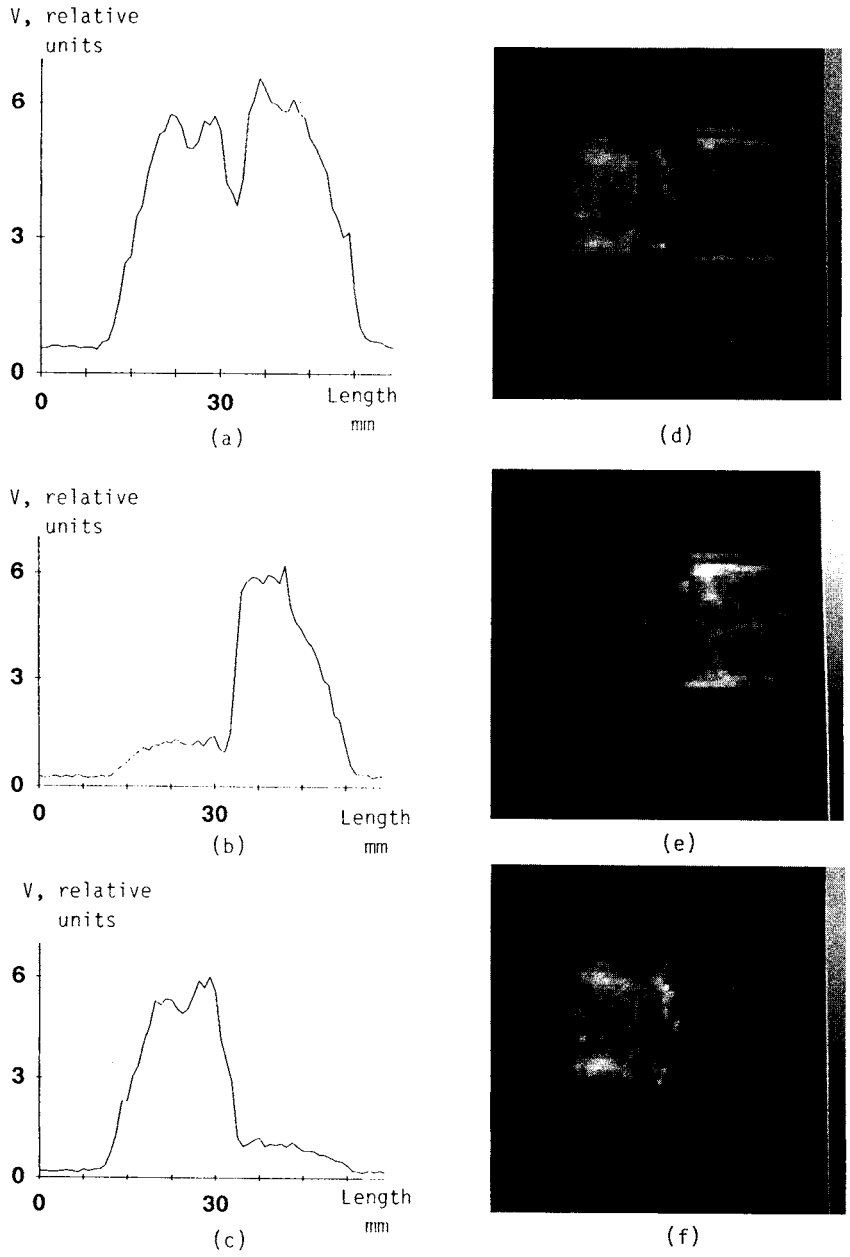

FIGURE 4 Halved core of Portland Limestone, one half saturated in n-decane, the other in water (a) total fluid profile; (b) oil profile; (c) water profile; (d) total fluid map; (e) oil map; (f) water map.

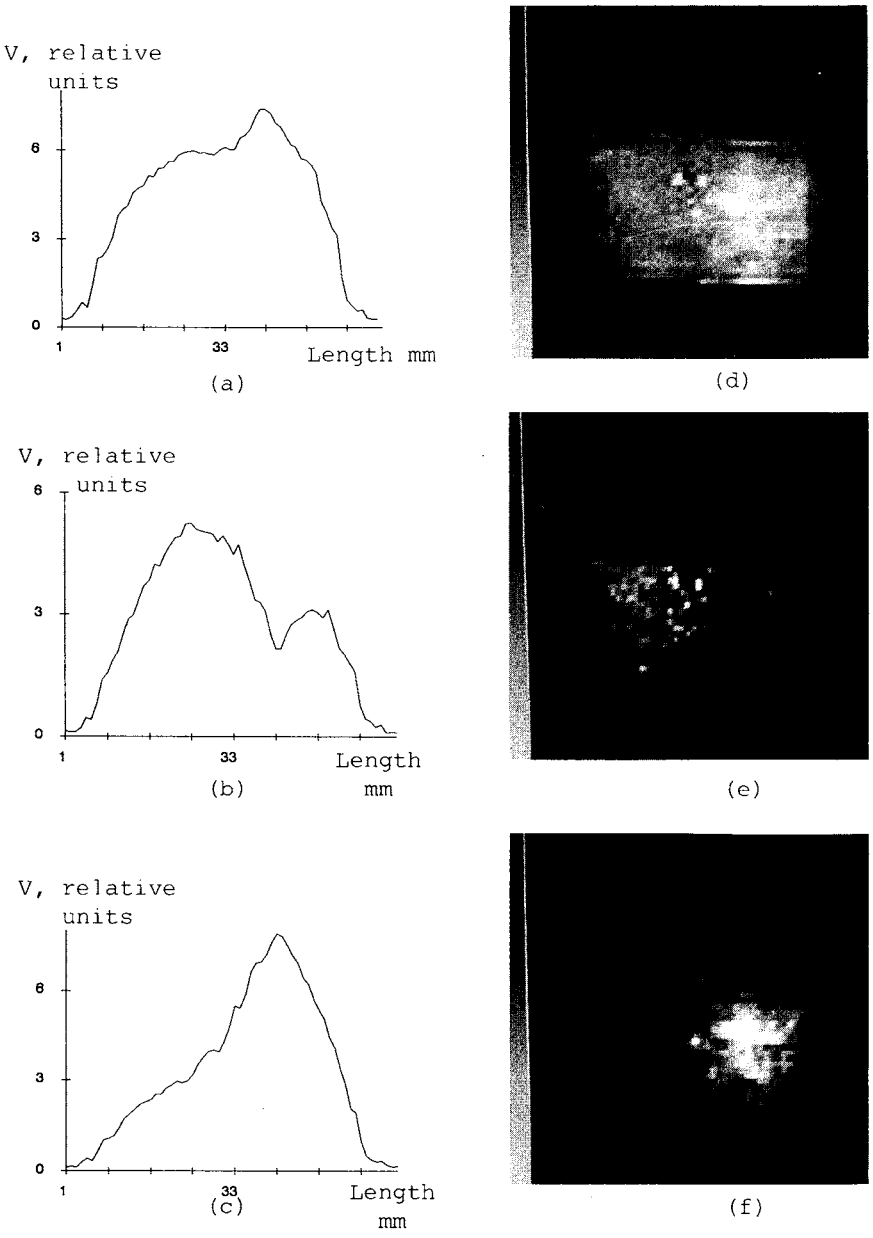

FIGURE 5 Glass bead pack injected with several PV water followed by 45% PV n-decane (a) total fluid profile; (b) oil profile; (c) water profile; (d) total fluid map; (e) oil map; (f) water map.

the beads. A globule of decane has preceded the injected oil and collected at the outlet end of the pack where a tissue barrier was used to retain the beads. This small quantity was resolved with both 1-D and 2-D CSI. This was confirmed by investigating the spectra from this area, an example from the 2-D data set is shown in pixel 4 (Figure 6).

In view of the length of time required with the present equipment to acquire a full 2-D image of the sample (about 4.5 hours), it is likely that notable fluid redistribution occurred due to capillary forces. However, 1-D imaging required only 4.5 minutes and hence could be used to follow the progress of an injection flood.

The Chemical Shift Imaging technique was next applied to a linear, low rate waterflood using a Portland limestone sample. The core plug was first coated with "Araldite" around the outside and non magnetic platens and flow tubing were installed. The core plug was next fully saturated under vacuum with a light paraffin (30cs viscosity) and placed in the rf coil inside the magnet. Outside the magnetic field, a 'PERFUSOR' pump and a pipette were connected to the core with flow tubing.

The core was then water flooded at a flow velocity of 10 cm/day. Progress of the flood front was monitored by 1-D CSI and the fluid production recorded with time. The distribution of the fluids was imaged in 2-D, just after water breakthrough, while the flow was stopped.

Water saturation data was calculated from individual spectra of all the pixels at given times and used to plot the water saturation profiles shown in Figure 7. Figure 8 shows the 2-D image of the core taken just after breakthrough. This image reveals strong channelling of the water phase even at such very low flow velocity. The image slice is 4.5 mm thick and the fluid may go in and out of the image plane. Several PV of water were flooded through the core, followed by several PV of paraffin to attain an initial water saturation. The water flood was repeated and the flood progress monitored as before. This time a steep fluid bank was not detected with the 1-D profiles. The 2-D maps showed the water had followed previous channelling routes, although flow appeared to be more diffuse. If the initial water saturation was mobile in the pore space then the relative permeability to water would be non-zero, so that there would exist a static flood capability to move water through the pore space.

The flood was continued to the residual oil saturation, the channelling was not altered.

The study was continued, with injection water being replaced by a 400 ppm Xanthan polymer solution. Figure 9 shows the image of a fluid bank generated in the core and the distinction between the species present.

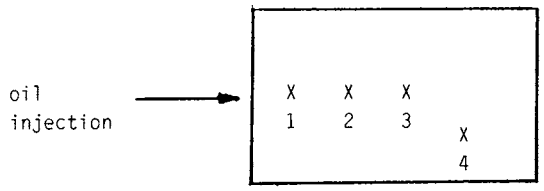

Schematic diagram ofthe position of the bead pack spectra

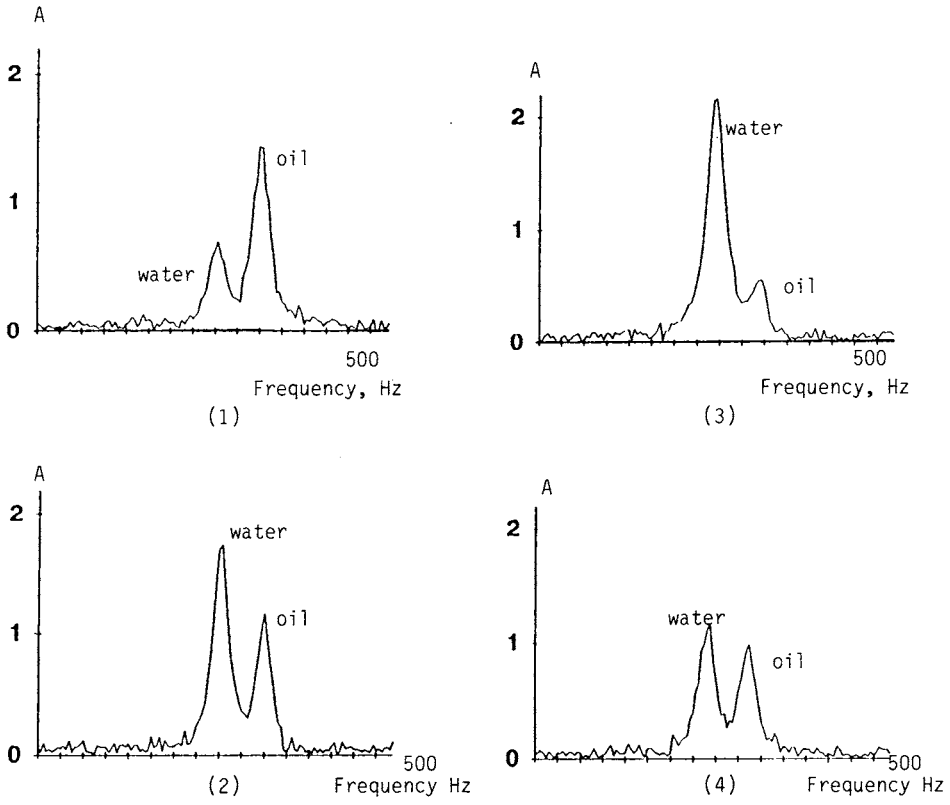

A = Amplitude, relative units

FIGURE 6 Example of chemical shift spectra from the 2-D chemical shift image of oil and water distributed in a glass bead pack.

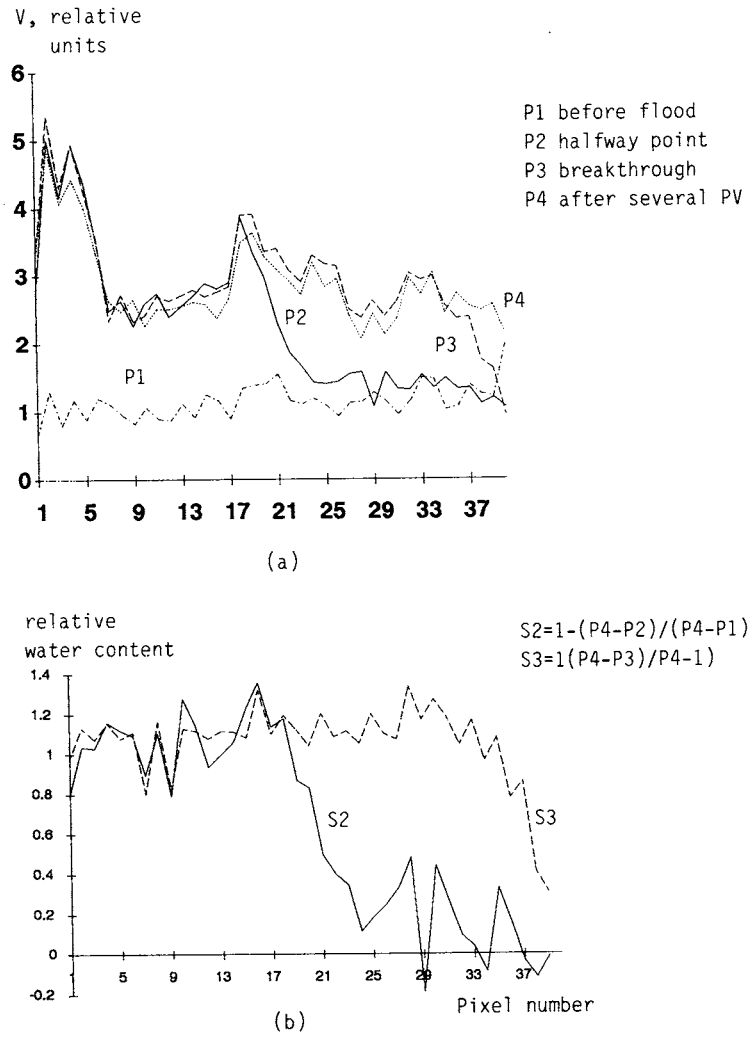

FIGURE 7 Core flood study Portland Limestone (a) water concentration profiles at various timepoints; (b) relative water content, calculated using P1 reference as 0% water content, and P4 as final water saturation in the presence of residual oil.

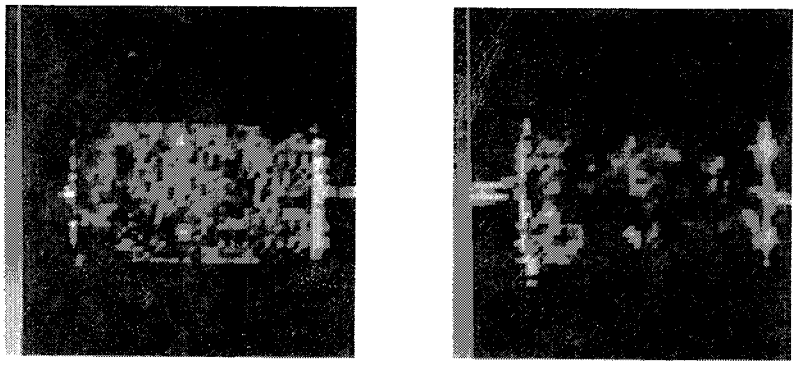

Oil map Water map

FIGURE 8 Oil and water maps of a Portland Limestone core 100% saturated with oil and injected with light paraffin (10cm/day) at breakthrough.

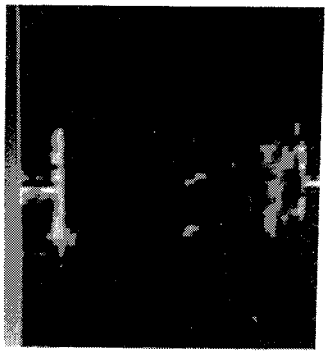

polymer injection

FIGURE 9 Water map of a Portland Limestone core showing a polymer solution bank generated by partial injection of 400ppm Xanthan (approx. 10% PV) with distributions of oil and water present.

The highest rate of flow that can be used without blurring the image depends on the imaging time. For our system 1-D imaging in 4.5 minutes gives a theoretical limit of 14 cm per day. Rapid imaging such as FLASH would allow the rate to be increased significantly.

CONCLUSIONS

The Chemical Shift MRI technique holds powerful promise in special core analysis where the saturation distribution within the core may be of interest. In our preliminary investigations we have shown that the porosity and the internal geometry of the pore space may be deduced from the fluid saturation images and that, with proper equipment selection, immiscible fluid distributions can be tracked in static and dynamic flow experiments. The technique appears to lend itself to fundamental observations of processes involving the competing displacement forces of capillarity, viscous flow and gravity. The limits of resolution of saturation at the individual pore level have not yet been explored but appear to be controlled largely by the power of the equipment employed.

The particular attributes of the technique that lend themselves to special core analysis research for petroleum engineering include the following:

- The rock matrix does not give a distinguishable liquid signal
- Signal is proportional to the concentration of each fluid
- Water and oil can be distinguished by their chemical shift.
- The fluid filled porosity and saturations can be measured.
- Wettability, and pore size affect relaxation rates T_1, T_2
- Imaging provides a way of spatially mapping these quantities providing experimental data for testing and analysis of simulation software.

APPENDIX

A.1. Principles of NMR

A.1.1. Relaxation Times

In the presence of an externally applied magnetic field $\underline{B}_0$ the summation of the individual nuclear spins gives the sample bulk nuclear magnetisation $\underline{M}$. At thermal equilibrium $\underline{M}$ will lie along the direction of the applied magnetic field $\underline{B}_0$. If a pulse of RF energy is applied at the resonant frequency, $\underline{M}$ will move through an angle away from the direction of $\underline{B}_0$ to a new position with components $\underline{M}_z$ along $\underline{B}_0$ and $\underline{M}_{xy}$ normal to $\underline{B}_0$. The $\underline{M}_{xy}$ component will rotate about the z direction (the direction of $\underline{B}_0$), at the resonant frequency. The oscillating electromagnetic field generated by the rotating components $\underline{M}_{xy}$ can be detected by a coil surrounding the sample with its axis normal to z direction. This nuclear magnetic resonance signal will be generated at the resonance frequency. It will decay with time due to the combination of three principal processes.

1. The transfer of energy from the spin system to the lattice with a characteristic exponential decay with time constant T_1 known as the spin-lattice relaxation time constant.
2. A random interaction between the nuclear spins which leads to a degeneration of coherence of the precession of spins which has a characteristic exponential time constant T known as the spin spin relaxation time constant.
3. In practice $\underline{B}_0$ is not perfectly homogeneous, this and the presence of any local magnetic field gradients will cause the spins to precess at slightly different frequencies so that there is a mutual dephasing which has a characteristic time constant T_2^*.

A.1.2. Measurement of Relaxation Times

The Inversion Recovery Sequence (180° - t - 90° - T_r) can be used to measure T_1 (Figure 10). An rf pulse $\alpha = 180^\circ$ is applied to the nuclear system at thermal equilibrium, the resulting magnetisation $\underline{M}$ will be tipped through 180° and lie along $-\underline{B}_0$ it will relax back to $\underline{B}_0$ exponentially in time according to equation A.1.1. where t is the time from the initial 180° pulse.

$$\underline{M}_z(t) = \underline{M}_0 \, (1 - 2 \exp(-t/T_1)) \qquad \text{(A.1.1)}$$

The magnetization $\underline{M}_z$ is parallel with the magnet field $\underline{B}_0$ so it does not generate a signal in the detection coil. To sample the magnetization $\underline{M}_z$, an $\alpha = 90^\circ$ rf pulse is applied at a time t after the 180°. This pulse tips the magnetization $\underline{M}_z$ into the xy plane, where it generates a signal in the

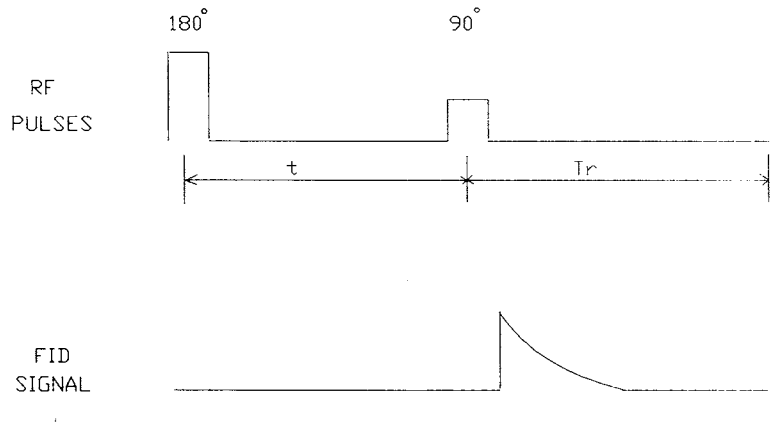

FIGURE 10 Typical rf pulses used for the inversion recovery sequence.

detection coil proportional to the value of $\underline{M}_z(t)$. The sequence is repeated with different values of t and the amplitude of the signal recorded. The sample magnetisation must be allowed to relax back to thermal equilibrium before the sequence can be repeated. The repetition time T_r is generally chosen to be greater than $5T_1$ at which time 99% of the magnetisation will have been re-established. The value of T_1 is calculated by fitting the values of $\underline{M}_z(t)$ to the exponential equation A.1.1.

In the absence of static field inhomogeneity, the transverse magnetization $\underline{M}_{xy}$, generated by application of an rf pulse, decays with the relationship:

$$\underline{M}_{xy} = M_0 \exp(-t/T_2) \qquad (A.1.2)$$

However, in the presence of inhomogeneities in the magnetic field the decay of the $\underline{M}_{xy}$ is characterized by T_2^* equation (A.1.3).

$$\underline{M}_{xy} = \underline{M}_0 \exp(-t/T_2^*) \qquad (A.1.3)$$

The dephasing after a 90° pulse due to the field inhomogeneities can be refocussed by application of a 180° pulse. This produces a signal echo. T_2 can be determined by measuring the peak amplitudes of a series of echoes, and exponentially fitting the data to Equation A.1.2. This

method was proposed by Carr, Purcell, Meiboom and Gill and is known as the CPMG sequence. The repetition time of the signal, T_r, must however allow for the equilibrium magnetisation to be re-established before the pulse sequence can be repeated. T_r is often chosen to be about $5T_1$.

T_2^* can be measured by recording the signal after an rf pulse and either fitting the data to equation A1.3 or by measuring the frequency bandwidth $\nu_{1/2}$ of the modulus NMR line and using equation A.1.4. The modulus lineshape is produced by Fourier transformation of the (time domain) signal)

$$\nu_{1/2} = \frac{\sqrt{3}}{\pi T_2^*} \qquad (A.1.4)$$

A.2. NMR Imaging

A.2.1. Imaging Methods

In order to obtain a two dimensional image of a three dimensional object it is necessary to define a slice through the object and then spatially encode this slice in both x and y directions. The spatially localised parameter can be assigned to a grey scale and the resulting image displayed. To encode spatial information into the signal magnetic field gradients are superimposed on the static magnetic field. These gradients can be used to spatially encode phase or frequency on the (time domain) NMR signal. This information is extracted by Fourier Transformation back to the spatial domain.

These essential elements are combined in a basic imaging pulse and gradient sequence. The technology development of NMR imaging is extensive. A good review is presented by Mansfield (1982).

A conventional 2-D Fourier Transform sequence (2DFT) is shown in Figure 11 (Edelstein, 1980). In the figure, each selective 90° pulse is followed at time $T_e/2$ by a non-selective 180° pulse. The 90° rf pulse is combined with the gradient G_z. The G_x gradient encodes spatial information in terms of NMR signal phase in the x direction, and is stepped through N values, where N is the number of rows of pixels in the image.

The G_y gradient encodes spatial information in terms of frequency in the y dimension of the sample. The pixel information is retrieved by a 2-D Fourier transformation in frequency (for y dimension) and phase (for x dimension).
The NMR signal echo is formed at T_e by a spin echo pulse sequence of 90° - $T_e/2$ -180°.

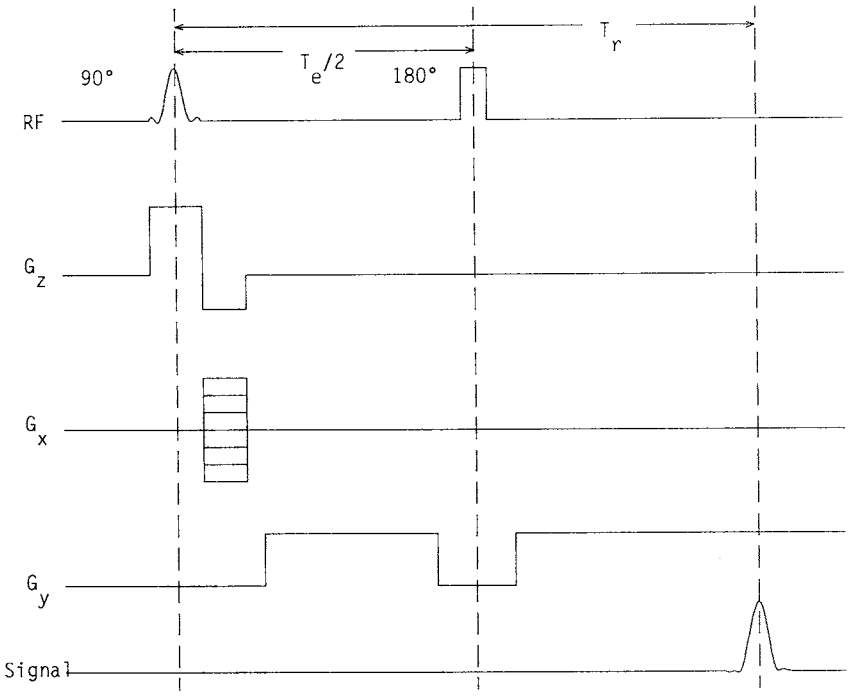

FIGURE 11 Spin echo pulse sequences in 2DFT

A.2.2. Chemical Shift Imaging (CSI)

Single phase fluid distributions are most effectively imaged using the 2DFT technique typically in a timescale of 2-4 minutes. For the quantitative separation of two phase distributions the CSI technique is more appropriate. The conventional 2DFT imaging technique will not permit the measurement of the chemical shift spectra as the frequency encoding gradient, applied during data collection, broadens the spectral lines so that molecular species specific information is lost. The solution implemented to overcome this problem utilises spatial phase encoding in both x and y directions by phase encoding (2DPE). The pulse sequence is shown in Figure 12.

Phase encoding pulses are used in both x and y directions in this figure, while homospoil gradients on the z direction are symmetric about the 180° rf pulse.

Slice selection is effected by a 90° selective rf pulse in

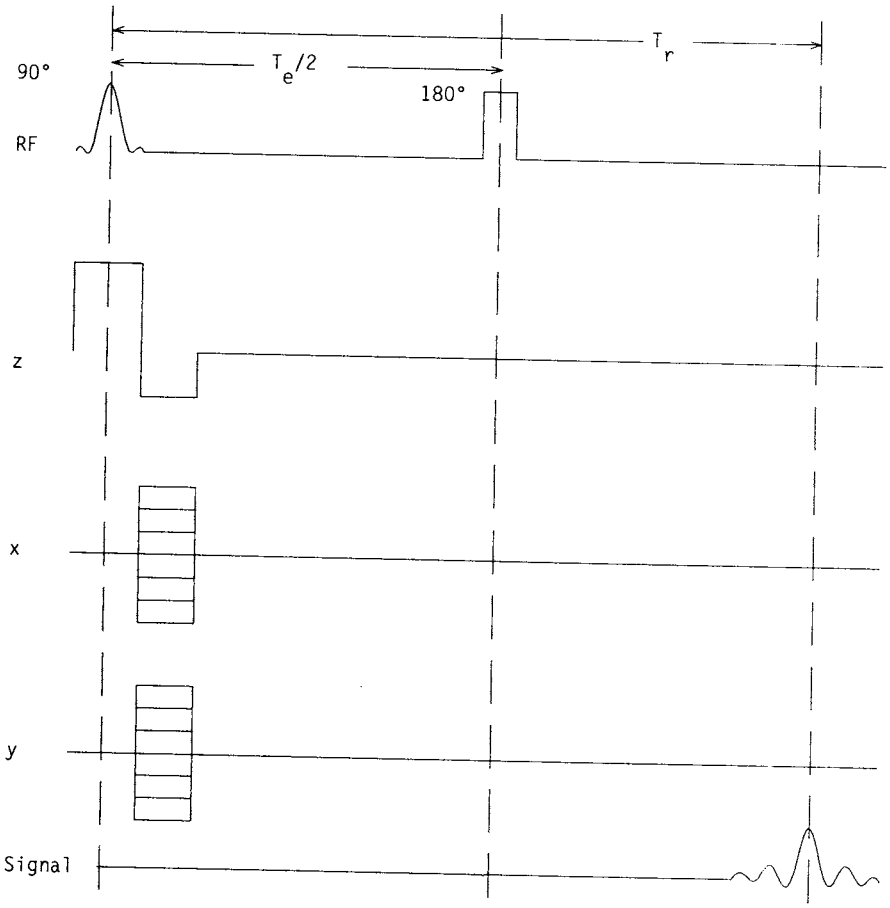

T_e = 40ms

T_r = 2000ms

FIGURE 12 Modified 2DPE sequence for chemical shift imaging

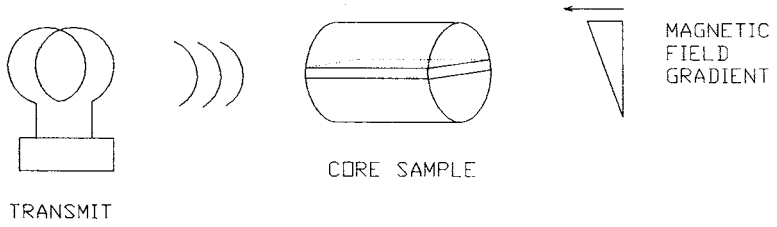

FIGURE 13 Slice selection by NMR

the presence of a G_z gradient Figure 13. During the evolution period a reversed gradient $-G_z$ is applied to refocus the excited magnetization. The use of a solenoid coil is generally preferred over saddle or other configurations from a signal to noise point of view. The solenoid coil must be oriented perpendicular to the static magnetic field, $\underline{B}_o$. The coil has been positioned parallel with the G_x direction so slicing along x produces a circular cross section through a cylindrical core, and slicing along y (or z) produces a longitudinal cross section. The slice position is determined by the centre frequency of the selective pulse, and the slice thickness by a combination of the bandwidth of the frequency components contained in the selective pulse and the applied gradient strength.

A slice selective rf pulse, gaussian weighted sync shape 1.5ms long, applied with a $2.5G/cm^{-1}$ gradient (G_z) gives a slice thickness of about 4mm. The phase encoding gradients are applied in the same time period as the rephase gradient.

The non selective 180^0 pulse generates out of plane image signal, this is removed by application of a homospoil gradient and phase cycling. The imaging sequence is repeated $2.n^2$ times where n is the number of pixels in x and y directions. The result is a 3-D data set with a chemical shift spectrum per image pixel, and there are n^2 pixels per image. The factor 2 arises from the phase cycling. The data can be displayed as a "picture" by integrating each pixel spectrum to produce one value per "picture" pixel. Figure 14 shows phase encoding schematically, and the resulting total fluid profile from integrating each pixel spectrum.

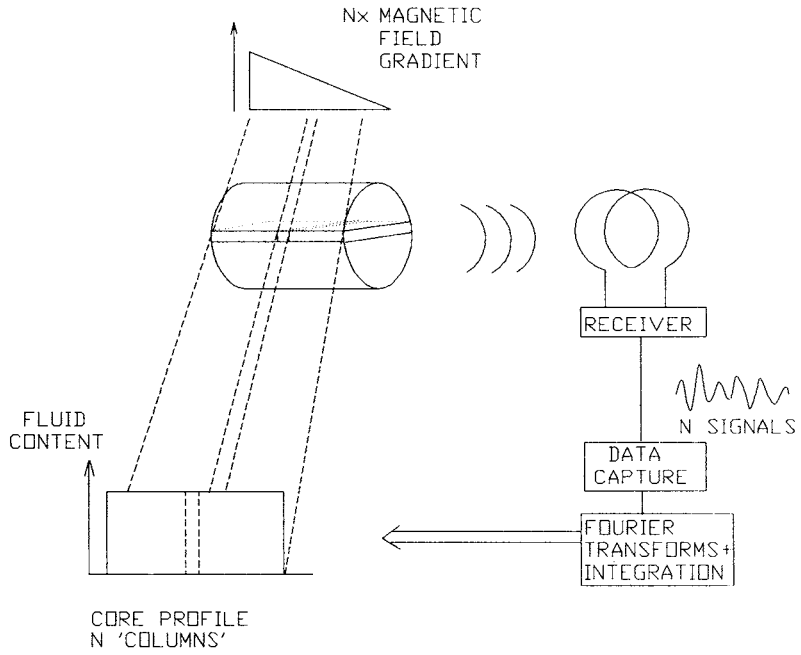

FIGURE 14 Phase encoding the NMR signal

The repetition time of the CSI technique is determined by T_1 and can be of the order of 2 secs. For a 64 x 64 image array the total imaging time would therefore be 4.5 hours. This is obviously only of use for static measurements. The increase of imaging rate is dependant on field strength and relaxation times. Full profile imaging may be unnecessary in order to track fluid movement in core plugs and selective imaging may prove adequate. There are electronically enhanced fast imaging techniques designed for medical applications (FLASH sequence, Haase et al 1986) but they require refinements to the imaging system to take advantage of significantly faster gradient switching times.

NOMENCLATURE

A	amplitude of spectral line
cs	centistroke
Hz	Hertz
md	Millidarcy
ms	Millisecond
ppm	Parts per million
PV	Pore Volume
T_1	Longitudinal relaxation time, ms
T_2	Transverse relaxation time, ms
T_2*	Relaxation rate due to magnetic field inhomogeneities.
V	Fluid concentration determined by NMR
$\nu_{1/2}$	Full width at half maximum height of a spectral line

ACKNOWLEDGEMENTS

The authors wish to thank their sponsors the Department of Energy. Also Rex Watt and Russell Simms of the Atomic Energy Authority, Winfrith for providing necessary materials and equipment; and Guiseppe Madinelli for his assistance.

REFERENCES

1. Abragam, A. (1961) *Principles of Nuclear Magnetism* OUP 1961
2. Archer J. S., Wall C. G. (1986) *Petroleum Engineering Principles and Practice*, Graham and Trotman 1986
3. Davis L.A. (1987) *VHF Electrical Measurements of Saturations in Laboratory Floods*. SPE8847 presented at Symposium on Enhanced Oil Recovery, Tulsa, April 20-23, 1987
4. Edelstein W.A., Hutchison J. M. S., Johnson G., Redpath T., (1980) *Spin warp NMR imaging and applications to human whole body imaging*. Physics in Medicine and Biology 25 No.4 July 1980 751-756.
5. Edelstein W. A., Vinegar H. J., Tutunjian P. N., Roener P.B., Mueller O. M. (1988). *NMR Imaging for Core Analysis* SPE18272 presented at the 63rd Annual Technical Conference and Exhibition of the Society of Petroleum Engineers, Houston, October 2-3, 1988.
6. Farrah T. C., Becker E. D. (1971) *Pulse and Fourier Transform NMR*, London, Academic Press.
7. Haase A., Frahm J., Matthaei D., Hanicke W., Merbolt K.D. (1986). *FLASH Imaging. Rapid NMR Using Low Flip-Angle Pulses*. Journal of Magnetic Resonance 67, 258-266.
8. Hall L. D., Rajanayagam V., Hall C. (1986) *Chemical-shift Imaging of Water and n-Dodecane in Sedimentary Rocks*. Journal of Magnetic Resonance 68, 185-188.
9. Hall L. D. Rajanayagam V., Hall C. (1987). *Chemical-shift Imaging of Oil and Water in Sandstone Rock at 80MHz*. Journal of Magnetic Resonance 74, 139-146.
10. Hove A.O., Ringen J.K., Read P.A. (1987). *Visualization of Laboratory Corefloods with the aid of Computerized Tomography of X-Rays*, SPE Reservoir Engineering, May 1987.
11. Josendal V.A., Sandiford B.B., Wilson J. W. (1952) *Improved Multiphase Flow Studies Employing Radioactive Tracers*, Transactions AIME 195, 65-76.
12. Kenyon W.E., Day P.I., Staley C., Willemsen J.F. (1986). *Compact and consistent representation of rock NMR data for permeability estimation*, SPE 15643, presented at 61st Annual Technical Conference and Exhibition of the Society of Petroleum Engineers, New Orleans, October 5-8, 1986.
13. Lauterbur P.C. (1973) *Image Formation by induced local interactions: Examples employing Nuclear Magnetic Resonance*. Nature 242 190-191.
14. Mansfield P., Morris P. G. (1982) *NMR Imaging in Biomedicine Supplement 2. Advances in Magnetic Resonance*. Editor Waugh J. Academic Press, New York, 1982.
15. McLauchlan K.A. (1972) *Magnetic Resonance*, Oxford Chemistry Series, Clarendon Press 1972.

16. Parsons R.W.(1975) *Microwave Attenuation - A new tool for monitoring saturations in laboratory flooding experiments.* Society of Petroleum Engineering Journal August 1975 302-309, Transactions AIME 259.
17. Robinson J.D., Loren J.D., Vajnar E.A., Hartman D.E. (1974). *Determining residual oil with the nuclear magnetism log.* Journal of Petroleum Technology 257, 226-236 1974.
18. Timur A. (1969). *Pulsed nuclear magnetic resonance studies of porosity, moveable fluid and permeability of sandstones.* Journal of Petroleum Technology 775-786.
19. Withjack E.M. (1987) *Computed tomography for rock-property determination and fluid-flow visualization.* SPE 16951 presented at the 62nd Annual Technical Conference and Exhibition of the Society of Petroleum Engineers, Dallas, September 27-30, 1987.